Inorganic Chemistry

Article

pubs.acs.org/IC

Solid State Isostructural Behavior and Quantified Limiting Substitution Kinetics in Schiff-Base Bidentate Ligand Complexes *fac*-[Re(*O,N*-Bid)$(CO)_3$(MeOH)]^n

Alice Brink, Hendrik G. Visser, and Andreas Roodt*

Department of Chemistry, University of the Free State, P.O. Box 339, Bloemfontein 9300, South Africa

Supporting Information

ABSTRACT: A range of *N,O*-donor atom salicylidene complexes of the type *fac*-[M(*O,N*-Bid)$(CO)_3$(L)]^n (*O,N*-Bid = anionic *N,O*-bidentate ligands; L = neutral coordinated ligand) have been studied. The unique feature of the complexes which crystallize in a monoclinic isostructural space group for complexes containing methanol in the sixth position (L = MeOH) is highlighted. The reactivity and stability of the complexes were evaluated by rapid stopped-flow techniques, and the methanol substitution by a range of pyridine type ligands indicates significant activation by the *N,O*-salicylidene type of bidentate ligands as observed from the variation in the second-order rate constants. In particular, following the introduction of the sterically demanding and electron rich cyclohexyl salicylidene moiety on the bidentate ligand, novel limiting kinetic behavior is displayed by all entering ligands, thus enabling a systematic probe and manipulation of the limiting kinetic constants. Clear evidence of an interchange type of intimate mechanism for the methanol substitution is produced. The equilibrium and rate constants (25 °C) for the two steps in the dissociative interchange mechanism for methanol substitution in *fac*-[Re(Sal-Cy)$(CO)_3$(MeOH)] (**5**) by the pyridine type ligands 3-chloropyridine, pyridine, 4-picoline, and DMAP are k_3 (s^{-1}), 40 ± 4, 13 ± 2, 10.4 ± 0.7, and 2.11 ± 0.09, and K_2 (M^{-1}), 0.13 ± 0.01, 0.21 ± 0.03, 0.26 ± 0.02, and 1.8 ± 0.1, respectively.

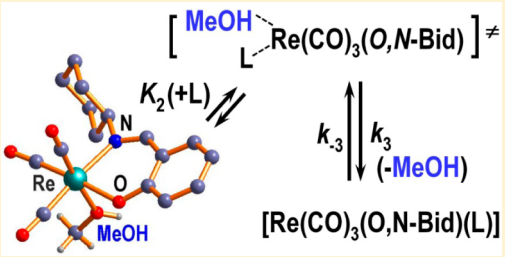

INTRODUCTION

Organometallic chemistry in aqueous solutions has been of considerable interest through the years with an expanding knowledge base, in particular in the fields of catalysis, green chemistry, and drug design.[1−8] The aqueous tricarbonyl complexes of the group 7 transition elements (Mn, Tc, and Re) have received particular attention due to the high kinetic stability of the carbonyl ligands in the low-spin d^6 *fac*-$[M(CO)_3]^+$ core.[9,10] The stability as well as the tendency to accept various bifunctional chelators containing different donor atoms have allowed the development of potential Re- and Tc-based radiopharmaceuticals to complexes with a low valent central metal core. For diagnostic nuclear medicine, ^{99m}Tc is still the most important radionuclide and represents roughly 80% of clinically administered radiopharmaceuticals.[11] Furthermore, Re may be utilized as a potential radiotherapeutic agent with its β^-emitting isotopes, ^{186}Re and ^{188}Re, as well as being a nonradioactive model for Tc.[12−14] The kinetic behavior of the aqueous *fac*-$[M(CO)_3]^+$ model complexes is an important aspect which may shed light into the synthesis, patient administration, uptake, and clearance of the radiopharmaceutical agents. To improve the understanding of the tricarbonyl complexes the mechanistic character of the reactivity of these type of organometallic complexes has to be extensively considered. Understanding the stability and reactivity of these new complexes in a controlled chemical environment may allow better understanding of behavior patterns in a biological environment. Knowledge gained will therefore assist in the design of optimum conditions for labeling.

The kinetic behavior of the water exchange and water substitution of *fac*-$[M(CO)_3(H_2O)_3]^+$ has been reported[4,15,16] and indicated that the ligand substitution mechanism was dependent on the nature of the entering ligand. With regards to *fac*-$[Re(CO)_3(H_2O)_3]^+$ complex formation, a mechanistic changeover occurs from interchange dissociative (I_d) for the ligands with harder character, to I_a for the ligands which have better nucleophilic properties and softer characteristics, of which dimetylsulfide and tertrahydrothiophene are good examples.

In order to subtly tailor the *fac*-$[M(CO)_3]^+$ complexes for use in radiopharmacy the [2 + 1] mixed ligand approach was proposed by Mundwiler et al.[17] The approach utilizes bidentate ligands to effectively occupy two of the three reactive aqua sites, thus leaving one site open for substitution. The lipophilicity, in this manner, can be gently manipulated by coordinating a biologically active molecule to either the entering monodenate ligand or the bidentate ligand backbone.[18,19] The countless possibilities of synthesis allows for the optimization of the properties and activity of model radiopharmaceuticals. The investigation into the substitution of *fac*-[M(*L,L′*-Bid)$(CO)_3(H_2O)]^{n+}$ (*L,L′*-Bid = neutral or monoanionic bidentate ligands) has become a focus of our research group as very few

Received: August 6, 2014
Published: November 13, 2014

Table 1. Comparison of Spectroscopic Data for *fac*-[Re(*N,O*-Bid)(CO)$_3$(L)] Complexes with L = Monodentate Ligands as Indicated

N,O-Bid compd	λ_{max} (nm)	ε (M^{-1} cm^{-1})	$\nu_{(CO)}$ (KBr; cm^{-1})		
[Re(Sal-Cy)(CO)$_3$(MeOH)][a]	293	14 210	2015		1872
[Re(5Me-Sal-3Me2Bu)(CO)$_3$(MeOH)][a]	382	1576	2016	1895	1872
[Re(5Me-Sal-*m*Tol)(CO)$_3$(MeOH)][a]	365	2124	2019	1923	1883
[Re(5Me-Sal-Hist)(CO)$_3$][b]	300	5206	2013	1903	1871
[Re(5Me-Sal-Trypt)(CO)$_3$(MeOH)][b]	262	8422	2014		1885
[Re(5Me-Sal-Trypt)(CO)$_3$(Py)][b]	382	2112	2016	1906	1882
[Re(5Me-Sal-Carba)(CO)$_3$(MeOH)][b]			2018		1892
[Re(5Me-Sal-Carba)(CO)$_3$(Py)][b]	286	30 960	2015	1909	1885
[Re(Sal-mTol)(CO)$_3$(MeOH)][c]	398	3139	2002		1869
[Re(Sal-mTol)(CO)$_3$(Py)][c]	402	2345	2015		1891
[Re(Sal-*p*Tol)(CO)$_3$(MeOH)][c]	386	2032	2020		1892
[Re(Sal-Ph)(CO)$_3$(MeOH)][c]	402	3717	2021		1893
[Re(Sal-Ph)(CO)$_3$(Py)][c]	407	2487	2015	1907	1889
[Re(Sal-3MeBu)(CO)$_3$(MeOH)][d]	383	1311	2001		1877
[Re(Sal-3MeBu(CO)$_3$(Py)][d]	389	2038	2014	1905	1878
[Re(Pico)(CO)$_3$(H$_2$O)][e]	313	5140	2022	1908	1874
[Re(2,4-dPicoH)(CO)$_3$(H$_2$O)][e]	339	4280	2035	1919	
[Re(2,4-dPicoH)(CO)$_3$(Py)][e]	315	5550	2030	1929	1908
[Re(2,4-dQuinH)(CO)$_3$(H$_2$O)][e]	352	51 900	2034	1936	1886
[Re(2,4-dQuinH)(CO)$_3$(Py)][e]	358	49 900	2024	1926	1869

[a]This work. [b]Reference 19. [c]Reference 22. [d]Reference 18. [e]Reference 20.

have previously been studied.[20,21] The substitution kinetics of the *fac*-[Re(*L,L′*-Bid)(CO)$_3$(H$_2$O)]$^{n+}$ complexes indicates interesting variations, for example, an *N,N′*-Bid positively charged metal complex has significant affinity for the negatively charged halide ligands, indicative of an associative mode of activation. For the *N,O*-Bid neutral metal complexes, the halide entering ligand is *ca.* 5−7 times faster than neutral entering ligands. For *O,O′*-Bid neutral metal complexes; in particular, a flavone complex, *fac*-[Re(Flav)(CO)$_3$(MeOH)] (Flav =3-hydroxy-flavonate), illustrates significant labilizing effect.[20] These unexpected labilizing effects were also found in a preliminary study for *N,O*-Bid neutral Schiff-base metal complexes and are of similar magnitude to that of the reported flavone complex.[22] The significant activation of the Schiff-base complex *fac*-[Re(Sal-T)(CO)$_3$(L)] (Sal-T = monoanionic *N,O*-salicylidene bidentate ligand; T = various functionalities coordinated to the imine N atom; L = coordinated monodenate ligands) was found to react rapidly according to a dissociative interchange mechanism. The use and reactivity of these salicylidene type complexes for radiopharmacy is of particular interest as it has been shown that biologically active substituents can readily be additionally coordinated to the *fac*-[Re(CO)$_3$]$^+$ core.[19] In general, all previous reports have indicated that the reactivity of the generally inert Re(I) metal center could be significantly altered and have opened numerous possibilities for the [2 + 1] approach.

In this Article, the solvent substitution behavior of *fac*-[Re(Sal-T)(CO)$_3$(L)] (L= methanol) is investigated, utilizing two sterically demanding aliphatic salicylidene bidentate ligands, namely, 2-(3-methylbutyliminomethyl)phenol (SalH-3MeBu) and 2-(cyclohexyliminomethyl)phenol (SalH-Cy), in conjunction with a systematic and chronologic range of coordinating ability entering ligands, while keeping the steric demand thereof constant. Only a small number of structures are reported in the literature for *fac*-[Re(*L,L′*-Bid)(CO)$_3$(MeOH)] complexes containing methanol solvent molecules as the sixth ligand. Thus, to enable better understanding of the dynamics and influence of the ligands on the Re-MeOH bond, the solid-state data available is increased by the three structures *fac*-[Re(Sal-Cy)(CO)$_3$(MeOH)], *fac*-[Re(5Me-Sal-3Me2Bu)-(CO)$_3$(MeOH)], and *fac*-[Re(5Me-Sal-*m*Tol)-(CO)$_3$(MeOH)], respectively, as reported here. An interesting structural correlation is observed for the *fac*-[Re-(*L,L′*)(CO)$_3$(MeOH)] complexes in general as the methanol solvent complexes as reported both here and in literature tend to crystallize isostructurally in one monoclinic space group, which will also be discussed.

RESULTS AND DISCUSSION

Synthesis. The *fac*-[Re(*N,O*-Bid)(CO)$_3$(MeOH)] complexes were successfully synthesized with methanol in the sixth position. Pure products were obtained from crystallization with reasonable yields. Attempts to synthesize the aqua complex, *fac*-[Re(*N,O*-Bid)(CO)$_3$(H$_2$O)], directly were unsuccessful and tend to favor the formation of product mixtures. During kinetic investigations, the complexes were noted to exchange the coordinated MeOH with the water in solvents which were not predried. Preliminary kinetic studies on the water substitution were conducted and will be the subject of future studies, with the subtle effect of pH significantly complicating the kinetics. Thus, utilizing methanol as a solvent instead of water proved highly successful and allowed the synthesis of crystallographically pure complexes.

In agreement with the [2 + 1] approach, the coordinated methanol is readily replaced by other noncharged ligands. Similarly, the coordinated functionality on the Schiff-base imine nitrogen could be altered from aromatic to biologically active, and now aliphatic synthons, and still allow successful coordination to the *fac*-[Re(CO)$_3$] core.[18,19] The successful formation of the *fac*-[Re(*L,L′*-Bid)(CO)$_3$(MeOH)] complexes could be easily confirmed by X-ray diffraction, ^{1}H and ^{13}C NMR, and IR spectroscopy. Crystallization at low temperature is essential for the formation of pure crystalline products;

dx.doi.org/10.1021/ic5019168 | *Inorg. Chem.* 2014, 53, 12480−12488

Table 2. Crystallographic Data of *fac*-[Re(Sal-Cy)(CO)$_3$(MeOH)] (5), *fac*-[Re(5Me-Sal-3Me2Bu)(CO)$_3$(MeOH)] (6), and *fac*-[Re(5Me-Sal-*m*Tol)(CO)$_3$(MeOH)] (7)

	5	6	7
empirical formula	$C_{17}H_{20}NO_5Re$	$C_{17}H_{22}NO_5Re$	$C_{19}H_{18}NO_5Re$
fw	504.55	506.56	526.54
cryst syst	monoclinic	monoclinic	orthorhombic
space group	*C*2/*c*	*C*2/*c*	*Pbcn*
a (Å)	18.096(4)	18.1040(4)	18.9720(7)
b (Å)	14.441(3)	15.1508(4)	14.2191(5)
c (Å)	13.753(3)	13.8715(4)	14.2316(5)
α (deg)	90	90	90
β (deg)	107.18(3)	102.896(2)	90
γ (deg)	90	90	90
V (Å^3)	3433.6(1)	3708.8(2)	3839.2(2)
Z	8	8	8
D_{calcd} (g cm^{-3})	1.952	1.814	1.822
μ (mm^{-1})	7.104	6.577	6.358
F(000)	1952	1968	2032
T (K)	100	100	100
λ (Å)	0.71073	0.71073	0.71073
cryst color	colorless	yellow	yellow
cryst morphology	cuboid	cuboid	cuboid
cryst size (mm^3)	0.24 × 0.16 × 0.16	0.30 × 0.17 × 0.15	0.41 × 0.16 × 0.15
θ range (deg)	1.84−28.00	1.77−28.00	1.79−28.00
completeness (%)	99.1	100.0	99.9
index ranges	h = −22 to 23	h = −23 to 23	h = −23 to 25
	k = −18 to 19	k = −20 to 20	k = −18 to 18
	l = −17 to 18	l = −18 to 18	l = −18 to 16
reflns collected	14 839	29 957	51 881
indep reflns	4107	4479	4643
R_{int}	0.0963	0.0338	0.0538
data/restraints/params	4107/0/217	4479/0/240	4643/0/218
GOF	1.027	1.295	1.168
R_1 [$I > 2\sigma(I)$]	R1 = 0.0760, wR2 = 0.1850	R1 = 0.0195, wR2 = 0.0645	R1 = 0.0353, wR2 = 0.0996
R_1 (all data)	R1 = 0.0983, wR2 = 0.2056	R1 = 0.0259, wR2 = 0.0947	R1 = 0.0714, wR2 = 0.1466
ρ_{max} and ρ_{min} (e Å^{-3})	7.337, −5.607	0.996, −1.183	1.703, −2.365

however, once formed, the complexes are stable for months provided it is stored under inert conditions.

Spectroscopy. The complexes all display characteristic UV−vis spectra typical of the low-spin d^6 Re(I) *fac*-tricarbonyl metal core, also when ligand substitution has been affected.[23] The infrared data reported show symmetric stretching bands in the same range as other similar Schiff base complexes (Table 1), and the carbonyl stretching frequencies agree with the electron density of the metal center as induced by the bidentate/monodentate ligand combination.[24−26] The ^{1}H NMR spectra of *fac*-[Re(5Me-Sal-*m*Tol)(CO)$_3$(MeOH)] and [Re(5Me-Sal-3Me2Bu)(CO)$_3$(MeOH)] complexes indicate rotamers for the nitrogen coordinated functionality similar to that previously found.[18] The imine carbon (C1) is situated around 170−160 ppm in ^{13}C NMR spectra. The IR data does not indicate whether or not *fac*-[Re(Sal-Cy)(CO)$_3$(MeOH)], *fac*-[Re(5Me-Sal-3Me2Bu)(CO)$_3$(MeOH)], and *fac*-[Re(5Me-Sal-*m*Tol)(CO)$_3$(MeOH)] are particular more electron-rich that the other *N*,*O*-Bid complexes listed in Table 1.

X-ray Crystallography. The crystal structures of complexes **5**, **6**, and **7** were determined by X-ray crystallography, and the data collection parameters, basic crystallographic data, and geometric parameters are summarized in Tables 2 and 3, respectively. The molecular geometries and structures of **5**, **6**, and **7** are illustrated in Figure 1a−c, respectively, while the atom numbering schemes are also indicated. The rhenium(I) to monodentate ligand bond distances are listed as Re−L in Table 3.

Table 3. Selected Bond Distances (Å) and Angles (deg) for 5, 6, and 7 (L = MeOH)

	5	6	7
Bond Distance			
Re1−N1	2.202(9)	2.179(4)	2.157(5)
Re1−O1	2.131(7)	2.117(3)	2.123(4)
Re1−C01	1.896(11)	1.916(5)	1.914(7)
Re1−C02	1.894(13)	1.903(4)	1.895(9)
Re1−C03	1.869(10)	1.896(5)	1.901(11)
Re1−L	2.172(8)	2.180(3)	2.189(5)
N1−C1	1.282(12)	1.285(6)	1.278(9)
Bond Angle			
N1−Re1−O1	84.6(3)	85.47(11)	83.77(19)
L−Re1-C03	174.9(3)	176.03(16)	175.7(3)
Re1−O04−C04	123.8(7)	123.1(3)	126.4(5)
Re1−C02−O02	175.8(10)	177.4(4)	178.7(8)
C1−N1−C21	113.6(9)	115.6(4)	116.8(6)
C22−C21−N1−C1	107.6(11)	100.3(6)	91.4(1)

The three complexes, **5**, **6**, and **7**, crystallized as distorted octahedra at the rhenium(I) center. Each rhenium atom is coordinated by three facial carbonyl ligands, an *N*,*O*-bidentate

dx.doi.org/10.1021/ic5019168 | *Inorg. Chem.* 2014, 53, 12480−12488

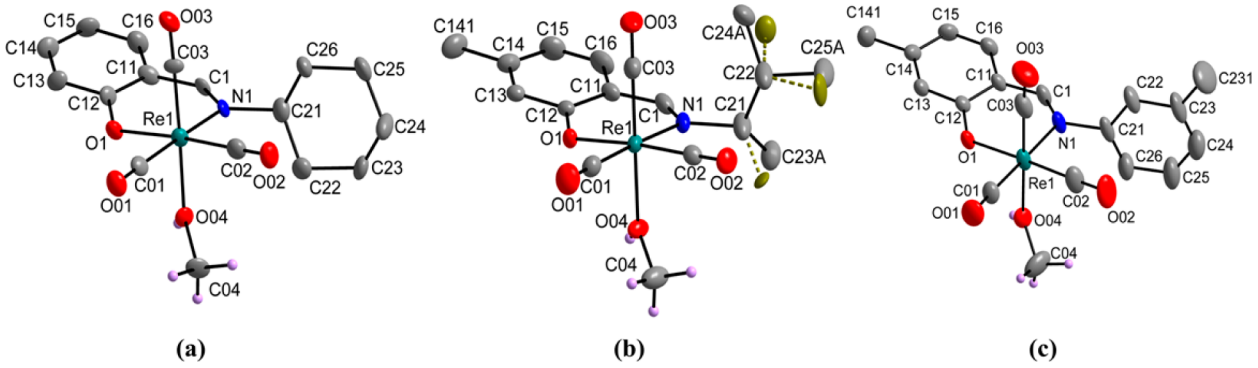

Figure 1. Molecular structures of the rhenium complexes (a) *fac*-[Re(Sal-Cy)$(CO)_3$(MeOH)] (**5**), (b) *fac*-[Re(5Me-Sal-3Me2Bu)$(CO)_3$(MeOH)] (**6**), (c) *fac*-[Re(5Me-Sal-*m*Tol)$(CO)_3$(MeOH)] (**7**). Only complexes indicated, H atoms (except for the methanol protons) are omitted for clarity.

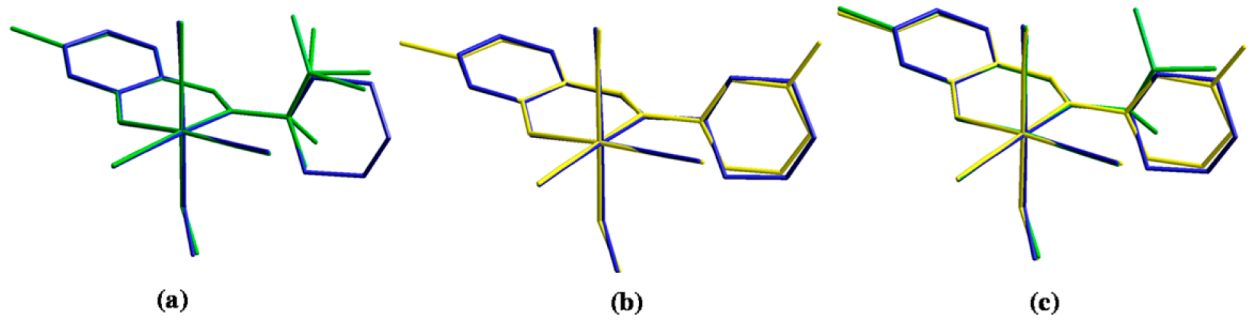

Figure 2. Graphical overlay of rhenium complexes. Overlays are not drawn through substituents coordinated to the N atom of the salicylidene backbone to allow free rotation of coordinated functionalities. (a) *fac*-[Re(Sal-Cy)$(CO)_3$(MeOH)] (**5**) (blue) and *fac*-[Re(5Me-Sal-3Me2Bu)$(CO)_3$(MeOH)] (**6**) (green; disorder indicated). (b) *fac*-[Re(Sal-Cy)$(CO)_3$(MeOH)] (**5**) (blue) and *fac*-[Re(5Me-Sal-*m*Tol)$(CO)_3$-(MeOH)] (**7**) (yellow). (c) *fac*-[Re(Sal-Cy)$(CO)_3$(MeOH)] (**5**) (blue), *fac*-[Re(5Me-Sal-*m*Tol)$(CO)_3$(MeOH)] (**7**) (yellow), and *fac*-[Re(5Me-Sal-3Me2Bu)$(CO)_3$(MeOH)] (**6**) (green; disorder not indicated).

moiety, and a neutral MeOH solvent molecule. The bidentate ligands each contain a different functionality at the imine nitrogen atom. Complexes **5** and **6** crystallize in the monoclinic space group, *C*2/*c*, both with one metal complex molecule in the asymmetric unit.

The two solid state structures are isostructural (similar structural parameters; all atoms in virtually the same positions throughout each structure) with each other as well as with four other previously published structures, *i.e.*, *fac*-[Re(Sal-3MeBu)-$(CO)_3$(MeOH)],[18] *fac*-[Re(Sal-*m*Tol)$(CO)_3$(MeOH)], *fac*-[Re(Sal-*p*Tol)$(CO)_3$(MeOH)], and *fac*-[Re(Sal-Ph)$(CO)_3$-(MeOH)].[22] There is a distinct tendency for these Schiff-base *fac*-[Re(Sal-T)$(CO)_3$(MeOH)] complexes which contain a coordinated methanol solvent molecule as sixth ligand to crystallize in the *C*2/*c* monoclinic space group. The only exception to date is complex **7** which has crystallized in the orthorhombic *Pbcn* space group. The reason for the isostructural behavior is not yet completely understood and is currently under investigation, but similar orientation of the imine substituent, provided its spacial demand is not that significantly different from the others, is expected to contribute to this (Figure 2).

The Re1−N1 bond distances [(**5**) 2.202(9) Å; (**6**) 2.179(4) Å; (**7**) 2.157(5) Å] and Re1−O1 bond distances [(**5**) 2.131(7) Å; (**6**) 2.117(3) Å; (**7**) 2.123(4) Å] are in good agreement with those reported in related systems, and it ranges from 2.093 to 2.184 Å for Re−O and 2.152−2.199 Å for Re−N.[20,27−29] The bite angles of the coordinated *N*,*O*-Bid ligand, N1−Re1−O1 [(**5**) 84.6(3)°; (**6**) 85.47(11)°; (**7**) 83.77(19)°], compare well with those of other 6-membered cyclic bidentate ligands and range from 79° to 86°. This is typically about 10° larger than that found in similar 5-membered *N*,*O*-bid ligand complexes. The Re−MeOH bond distances (Re−O04) [(**5**) 2.172(8) Å; (**6**) 2.180(3) Å; (**7**) 2.189(5) Å] are similar to that in the *fac*-[Re(Flav)$(CO)_3$(MeOH)] (2.204(4) Å) and the *fac*-[Tc-(*NN*′)$(CO)_3$(MeOH)]$^+$ complex[30] (*N*,*N*′ = 2.1773 Å). The Re−CO bond distances in complexes **5**, **6**, and **7** agree well with this.

Substitution Kinetics. The methanol substitution reactions between *fac*-[Re(*L*,*L*′-Bid)$(CO)_3$(MeOH)] and various neutral monodentate entering ligands were monitored in methanol as solvent. The poor solubility of some complexes in water excluded the use thereof, and to ensure the integrity of the coordinated methanol, pure methanol was used. Freshly distilled, dry methanol is essential to minimize slow water exchange, as observed in reagent grade methanol which contained water.

A chronologic range of different substituted pyridines (3-chloropyridine, pyridine, 4-picoline, and 4-dimethylaminopyridine) was selected as the monodentate entering ligands specifically for their systematic increase in basiscity as manifested in their reported pK_a values (2.81, 5.23, 5.99, and 9.8).[31,32]

The substitution of the coordinated methanol may proceed via three different activation processes as depicted in Scheme 1.

Bromide ions (as NaBr or $[Et_4N]Br$) as potential entering ligands were evaluated in preliminary kinetic experiments, but no reaction could be detected. This is in agreement with previous synthetic experiments which showed that all Br^- species are replaced by methanol from $[Et_4N]_2[Re(CO)_3(Br)_3]$

dx.doi.org/10.1021/ic5019168 | *Inorg. Chem.* 2014, 53, 12480−12488

Scheme 1. Substitution of Coordinated Methanol from *fac*-[Re(*O,N*-Bid)(CO)$_3$(MeOH)] by Pyridine Type Ligands (L) via an Associative (A), Dissociative (D), or Interchange (I) Process, According to Basolo and Pearson[33]

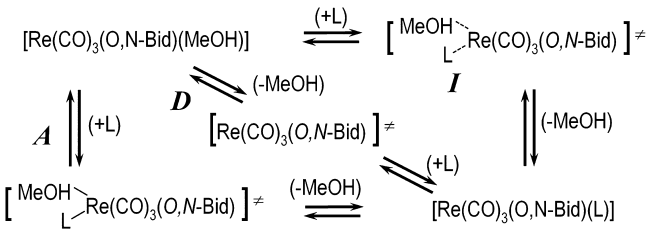

upon introduction of the SalH ligands when using MeOH as solvent. UV−vis experiments on all complexes and ligands indicated no detectable decomposition for several days and, thus, stability in solution for the kinetic time span utilized in this study.

First-order plots were obtained for all reactions wherein the coordinated methanol was substituted by the entering pyridine type ligand, and were treated to obtain the pseudo-first-order rate constant as described earlier.[20,21] Plots of k_{obs} versus [Ligand] for the reactions utilizing various ligands are provided in Figures 3 and 4. Upon fitting the k_{obs} versus [Ligand] data to

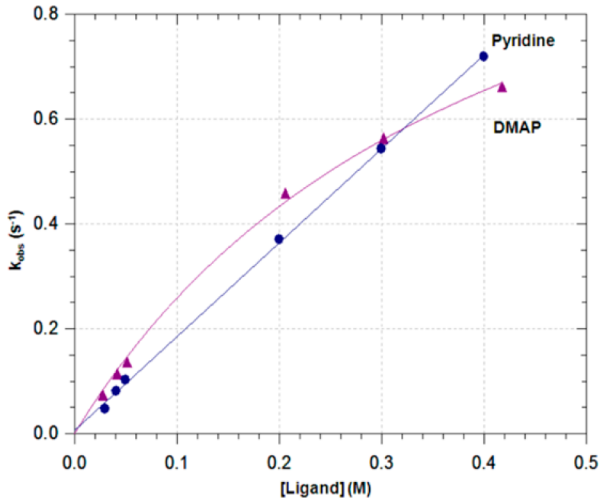

Figure 3. Plot of k_{obs} vs entering ligand for the reaction of *fac*-[Re(Sal-3MeBu)(CO)$_3$(MeOH)] and different entering ligands at 25.0 °C in methanol yielding limiting and linear relationships; [Re complex] = 3.22 × 10^{-4} M (pyridine λ = 416 nm, DMAP λ = 422 nm).

eqs 2, 4, and 5 as obtained by utilizing pseudo-first-order reaction conditions for the individual runs (ligand in excess), the individual rate constants as given in Table 4 were obtained. The rapid nature of the substitution reactions necessitated all kinetic measurements to be monitored on a stopped-flow spectrophotometer, and these were reproducible in both the rapid-scan (diode-array) and photomultiplier mode.

The k_{obs} versus [L] (entering ligand) plots, obtained for complexes **4** and **5**, produced either linear or nonlinear plots. For pseudo-first-order conditions with [L] ≫ [Re], only one reaction was observed for all the reagents under the reaction conditions described. It was hypothesized that the steric bulk of the aliphatic complexes *fac*-[Re(Sal-3MeBu)(CO)$_3$(MeOH)] (**4**) and *fac*-[Re(Sal-Cy)(CO)$_3$(MeOH)] (**5**) may affect the

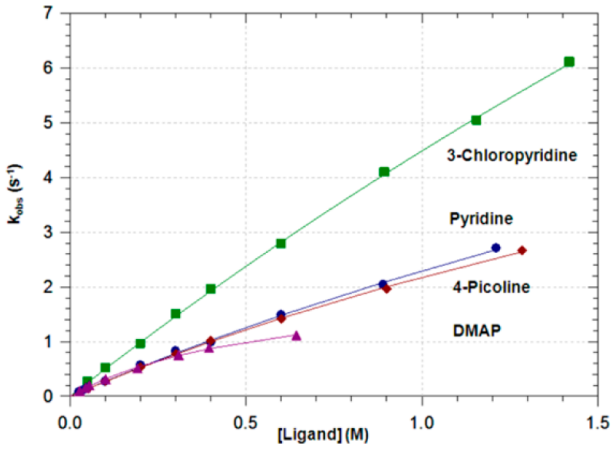

Figure 4. Plot of k_{obs} vs entering ligand for the reaction of *fac*-[Re(Sal-Cy)(CO)$_3$(MeOH)] and different entering ligands at 25.0 °C in methanol yielding limiting relationships; [Re complex] = 1.83 × 10^{-4} M (3-chloropyridine λ = 419 nm; pyridine λ = 417 nm; 4-picoline λ = 418 nm; DMAP λ = 420 nm).

substitution rates relative to the rates reported for planar aromatic functionalities.[22]

The substitution of methanol in the aliphatic complex *fac*-[Re(Sal-3MeBu)(CO)$_3$(MeOH)] (**4**) with various concentrations of 4-dimethylaminopyridine (DMAP) and pyridine (Py) was investigated at 25.0 °C. For the substitution reaction with DMAP, nonlinear plots were obtained whereas a linear relationship was obtained for the reaction with pyridine, see Figure 3.

This tendency follows the pattern found for the aromatic *fac*-[Re(*L,L′*-Bid)(CO)$_3$(MeOH)] complexes previously reported where an interchange dissociative mechanism was postulated.[22]

The methanol substitution reaction of the cyclic aliphatic complex *fac*-[Re(Sal-Cy)(CO)$_3$(MeOH)] (**5**) was then investigated at 25.0 °C, initially only with pyridine and DMAP as in other examples. Unexpectedly, line curvature was also found for *pyridine* as entering ligand which until this point has always given linear plots with various *fac*-[Re(*L,L′*-Bid)(CO)$_3$(MeOH)] at high concentrations. This led to the investigation being expanded to include a range of pyridine type ligand [3-chloropyridine, pyridine, 4-picoline, and 4-dimethylaminopyridine (pK_a values 2.81, 5.23, 5.99, and 9.8)][30,31] which exhibited a significant range of electron donating capabilities as manifested by their respective pK_a values, yet their steric contributions are expected to remain virtually constant. Nonlinear relationships were thus obtained for all four ligand reactions, but the extent of the plateau and the corresponding (curved) influence thereupon, and the individual stepwise influence, could also be quantified. Figure 4 illustrates the good fit of the data to eq 2; the curved nature utilizing the exact fits is however further highlighted in Figure 5.

From the previous studies of *fac*-[Re(Sal-*m*Tol)(CO)$_3$(MeOH)],[22] an interchange dissociative mechanism was proposed which yields limiting kinetics at high ligand concentrations. The rate equation for the interchange mechanism however predicts linear second-order rate behavior at low ligand concentrations, i.e., $k_f = k_1 = k_3K_2$. The rate constant for the forward reaction (k_f) for an *I* mechanism is therefore expected to closely resemble the "observed" second-order rate constant (k_1), especially at low ligand concentrations where saturation limits have not yet been reached. Rate

dx.doi.org/10.1021/ic5019168 | Inorg. Chem. 2014, 53, 12480−12488

Table 4. Rate Constants Determined for the Reaction of *fac*-[Re(*L*,*L*′-Bid)(CO)$_3$(MeOH)] with Different Entering Ligands at 25.0 °C in Methanol[a]

ligand	pK_a[b]	k_1 (M^{-1} s^{-1})	k_{-1} (s^{-1})	K_1 (M^{-1})	k_3 (s^{-1})	K_2 (M^{-1})	$k_f = k_3K_2$ (M^{-1} s^{-1})
fac-[Re(Sal-3MeBu)(CO)$_3$(MeOH)]							
pyridine	5.23	1.79 ± 0.02	0.006 ± 0.005	301 ± 256	11 ± 6	*0.17* ± 0.09	2 ± 1
DMAP	9.8				1.34 ± 0.09	2.4 ± 0.3	3.2 ± 0.5
fac-[Re(Sal-Cy)(CO)$_3$(MeOH)]							
3-chloropyridine	2.81	4.30 ± 0.06	0.14 ± 0.05	31 ± 9	40 ± 4	0.13 ± 0.01	5.1 ± 0.8
pyridine	5.23	2.22 ± 0.05	0.07 ± 0.03	30 ± 10	13 ± 2	0.21 ± 0.03	2.8 ± 0.6
4-picoline	5.99	2.03 ± 0.06	0.13 ± 0.04	16 ± 5	10.4 ± 0.7	0.26 ± 0.02	2.8 ± 0.3
DMAP	9.8	1.7 ± 0.1	0.13 ± 0.04	13 ± 5	2.11 ± 0.09	1.8 ± 0.01	3.7 ± 0.3

[a]Values with large ESD's (*indicated in italics*) are given for completeness of study. *fac*-[Re(Sal-3MeBu)(CO)$_3$(MeOH)] = 3.22 × 10^{-4} M, [pyridine] = 0.02−0.4 M, [DMAP] = 0.02−0.4 M; *fac*-[Re(Sal-Cy)(CO)$_3$(MeOH)] = 1.83 × 10^{-4} M, [3-chloropyridine] = 0.05−1.5 M, [pyridine] = 0.02−1.2 M, [4-picoline] = 0.05−1.3 M [DMAP] = 0.02−0.7 M. [b]References 30 and 31.

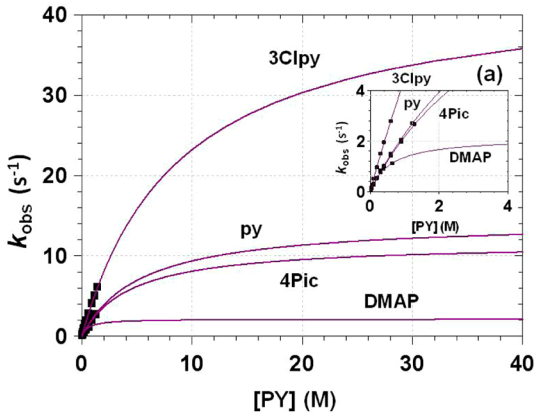

Figure 5. Extrapolated plot of k_{obs} vs concentration of pyridine type entering ligand ([PY]) for the reaction of *fac*-[Re(Sal-Cy)(CO)$_3$(MeOH)] and different entering ligands at 25.0 °C in methanol illustrating plateaus in limiting relationships; [Re complex] = 1.83 × 10^{-4} M (3-chloropyridine λ = 419 nm; pyridine λ = 417 nm; 4-picoline λ = 418 nm; DMAP λ = 420 nm). Inset a: Illustration of extrapolation of relative difference at intermediate higher concentrations.

constants obtained for complexes **4** and **5** clearly illustrate the similarity in k_f and k_1 in Table 4. An important observation, especially assuming an interchange *dissociative* mechanism, is however expected in a gradual variation in the pre-equilibrium constant (K_2), and should agree with the Bronsted acid/base properties of the pyridine type ligand, *i.e.*, reflecting electron density of the N atom on the entering entity. The K_2 constant does in fact increase by more than an order of magnitude from 3-chloropyridine to DMAP for complex **4**. The second-order rate constants (k_3), on the other hand, exhibit an inverse relationship to the Bronsted pK_a values of the entering pyridines.

The trend is similar to the tendency observed for *fac*-[Re(Sal-*m*Tol)(CO)$_3$(MeOH)].[22] The overall second order rate constants (k_1) obtained for the reaction of **4** and **5** with pyridine (k_1 = 1.79(2) M^{-1} s^{-1}; k_1 = 2.22(5) M^{-1} s^{-1}) is significantly faster than values determined for other analogous *N*,*O*-bidentate ligands[20] {*fac*-[Re(Quin)(CO)$_3$H$_2$O)] k_1 = 3.9(1) × 10^{-3} M^{-1} s^{-1}; *fac*-[Re(Pico)(CO)$_3$(H$_2$O)] k_1 = 1.6(1) × 10^{-3} M^{-1} s^{-1}; *fac*-[Re(2,4-QuinH)(CO)$_3$(H$_2$O)] k_1 = 3.31(2) × 10^{-3} M^{-1} s^{-1}; *fac*-[Re(2,4-PicoH)(CO)$_3$(H$_2$O)] k_1 = 1.641(8) × 10^{-3} M^{-1} s^{-1}; where Quin = 2-quinolinate, Pico = 2-picolinate, 2,4-QuinH = 2,4-quinolinedicarboxylate, 2,4-PicoH = 2,4-pyridinedicarboxylate, respectively}. The overall second-order rate constants (k_1) obtained for the reaction of **4** and **5** with pyridine are comparable to that determined for the labile methanol complex *fac*-[Re(Flav)(CO)$_3$(MeOH)] (k_1 = 1.38(8) M^{-1} s^{-1}) and water substitution for thiocyanate as entering ligand in related *O*,*O* complexes,[21] *fac*-[Re(Trop)-(CO)$_3$(H$_2$O)] (k_1 = 2.54(3) M^{-1} s^{-1}, Trop = tropolonato). The second-order rate constants of the salicylidene rhenium tricarbonyl complexes clearly indicate the significant labilizing effect which the *N*,*O* bidentate ligand has on the *fac*-[Re(CO)$_3$]$^+$ core.

The net interaction of the pyridine type ligand with the metal center during the overall steps in the *dissociative interchange* mechanism in this study is illustrated in more detail in Figure 5, where the clear plateau of the DMAP is reached much earlier than that of the other less electron rich pyridines, 4-picoline, pyridine, and in particular 3-cloropyridine. This is also emphasized by inset a in Figure 5, wherein a lower entering ligand range is considered, underlining the difference in behavior of the ligand range, but still illustrating the good nonlinear least-squares fits to eq 2 which the four respective data sets yielded.

Upon closer investigation of the different contributions to the *dissociative interchange* activated state, as defined in eq 1, the very rare observation shown in Figure 6 is highlighted. When the individual logarithmic contributions of the rapid association equilibrium, as defined by K_2, are plotted against the pK_a of the entering pyridine type ligand, a *nonlinear* relationship is obtained, see Figure 6a. However, when the logarithmic contribution of the rate-determining dissociation of the methanol from the activated state is considered, defined by k_3 (see Figure 6b), a *linear* relationship but opposite to that in part a is clearly seen. Moreover, when the two separate steps are *combined* as illustrated in Figure 6c, an excellent linear free energy relationship is obtained. This defines $pK_{a(PY)} \propto k_f = k_3K_2$, and the LFER [$\log(pK_{a(PY)}) \propto \log(k_3) + \log(K_2)$] is thus clearly indicating a similar intimate exchange mechanism for the range of pyridine ligands concerned, albeit for only four entering ligands. The subtle manipulation of the associated equilibrium and rate constants is emphasized.

Further research to further describe this observation is currently pursued to broaden the observation and define it more quantitatively.

■ CONCLUSION

The effects of the *N*,*O*-salicylidene bidentate ligands on the reactivity of the *fac*-[Re(CO)$_3$]$^+$ core were illustrated with the use of bulky aliphatic substituents coordinated to the bidentate backbone. Few rhenium and technetium tricabonyl complexes

dx.doi.org/10.1021/ic5019168 | *Inorg. Chem.* 2014, 53, 12480−12488

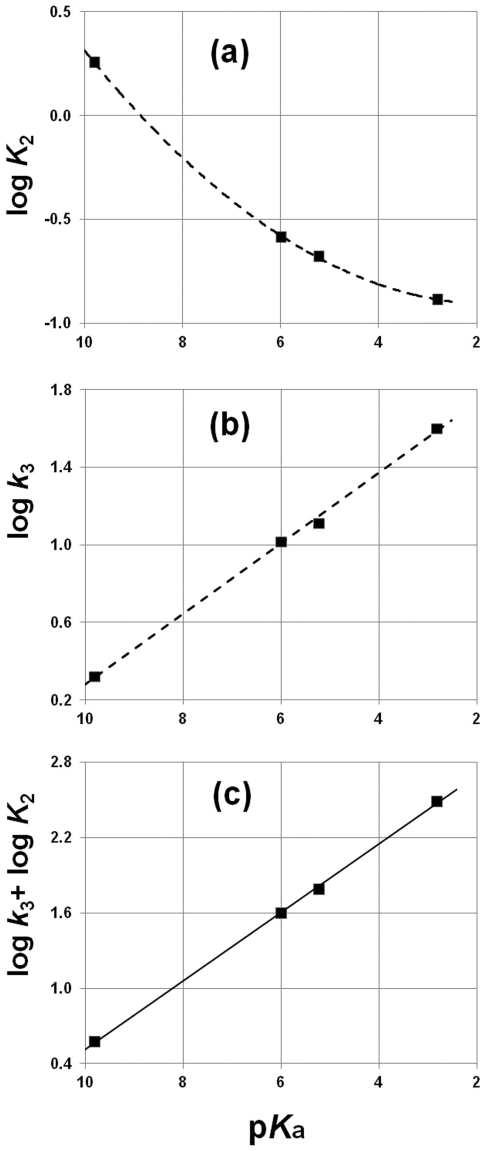

Figure 6. Plot of logarithmic relationships vs pK_a of pyridine ligands for (a) log K_2 vs pK_a; (b) log k_3 vs pK_a; (c) (log K_2 + log k_3) vs pK_a; for the reaction of *fac*-[Re(Sal-Cy)$(CO)_3$(MeOH)] and different entering ligands at 25.0 °C in methanol yielding limiting relationships; [Re complex] = 1.83 × 10^{-4} M (3-chloropyridine λ = 419 nm; pyridine λ = 417 nm; 4-picoline λ = 418 nm; DMAP λ = 420 nm).

containing either the salicylidene bidentate ligand or coordinated methanol in the sixth position have ever been reported. Even fewer contain both combinations wherein the kinetic mechanistic effects of *fac*-[Re(*L*,*L*′-Bid)$(CO)_3$(MeOH)] have been investigated. The X-ray diffraction studies of *fac*-[Re(*L*,*L*′-Bid)$(CO)_3$(MeOH)] illustrate the unusual tendency of the salicylidene methanol coordinated metal crystal structures to crystallize isostructurally in the *C*2/*c* space group. On the other hand, kinetic studies confirmed the significant activation of the salicylidene Re(I) metal center, comparable to other *O*,*O*′-bidentate complexes investigating the methanol and water substitution of the sixth position. In particular, the net effect of different steps in the dissociative interchange substitution for the methanol substitution allowed the rare opportunity to analyze and correlate the electron donating ability of the entering pyridine type ligands directly with the total activation pathway and the separate steps therein. These complexes are exciting prospects for the [2 + 1] labeling method, which needs to be expanded and broadened under aqueous conditions to allow radiolabeling of Tc-99m.

EXPERIMENTAL SECTION

General. Double distilled methanol and water were used in all experiments, which were performed aerobically. All chemicals (reagent grade) as utilized were purchased from Sigma-Aldrich unless otherwise noted. *fac*-$[NEt_4]_2[ReBr_3(CO)_3]$ was synthesized as previously reported[34,35] using rhenium pentacarbonyl bromide as reactant obtained from Strem Chemicals, Newburyport, MA.

The ligands, 2-(cyclohexyliminomethyl)phenol (SalH-Cy) (**1**), 5-methyl-2-(1,2-dimethylpropyliminomethyl)phenol (5Me-SalH-3Me2Bu) (**2**), and 5-methyl-2-(*m*-tolyliminomethyl)phenol (5Me-SalH-*m*Tol) (**3**), as well as *fac*-[Re(Sal-3MeBu)$(CO)_3$(MeOH)] (**4**) were synthesized according to literature procedures.[18,36,37] The ^{1}H and ^{13}C Fourier-transformed NMR spectra were recorded at 25 °C at 600.28 and 150.96 MHz, respectively, on a Bruker AXS 600 MHz spectrometer in CD_3OD (3.31 ppm), C_3H_6O (2.05 ppm), and $CDCl_3$ (7.26 ppm), with chemical shifts given in ppm. ^{13}C NMR spectra were referenced to the ^{13}C resonances for CD_3OD (49.0 ppm), C_3H_6O (29.8 ppm), and $CDCl_3$ (77.2 ppm). Infrared spectral data were recorded at ambient temperature (22 ± 2 °C) on a Bruker (Tensor 27) spectrophotometer spanning a laser range 4000−370 cm^{-1}. Spectra from solid samples were recorded as KBr pellets while liquid samples (methanol solution) were obtained in a sodium chloride liquid cell with a constant temperature cell regulator, accurate to within 0.3 °C. UV−vis spectra were obtained on a Varian Cary 50 Conc spectrophotometer in 1.000 ± 0.001 cm quartz cuvette cells. The temperature was regulated by a Julabo F12-mV unit, accurate to ±0.05 °C.

Rapid kinetic reactions with half-lives shorter than 20 s were monitored at constant temperature (accurate within 0.05 °C) on a Hi-Tech (SF-61DX2) stopped-flow spectrophotometer attached to a Julabo F12-mV temperature regulator as mentioned above. The third generation stopped-flow system has a thermostated SHU61DX sample handling unit and can be operated in the diode-array mode with a dead time <5 ms, yielding 400 nm spectral width scans at <5 ms/complete scan, for collecting initial reaction data to assess the appropriate wavelengths for monitoring the reactions studied at the largest absorbance changes. After selection of the appropriate wavelength(s), the SF system was switched to the photomultiplier mode (more sensitive; dead time at 25 °C *ca.* 1 ms) to study the actual individual kinetic reactions. The kinetic data points reported per concentration represent an average of 4 individual traces.

***fac*-[Re(Sal-Cy)$(CO)_3$(MeOH)] (5).** $[NEt_4]_2[ReBr_3(CO)_3]$ (0.100 g, 0.130 mmol) was dissolved in methanol (10 mL) followed by the addition of silver nitrate (0.0661 g, 0.389 mmol). The reaction mixture was stirred for 26 h at room temperature, followed by the removal of the precipitated AgBr by filtration. The SalH-Cy ligand (0.0277 g, 0.136 mmol) was subsequently dissolved in methanol and added dropwise to the above solution. The reaction mixture was heated at 70 °C (while stirring) for 12 h. The bulk of the solvent was then removed under reduced pressure, yielding crystals (suitable for single crystal X-ray analysis) upon slow cooling to 5 °C. (Yield of the crystalline product: 0.0582 g, 89%.)

IR (KBr, cm^{-1}): $\nu_{(CO)}$ 2015, 1872. UV−vis (nm, M^{-1} cm^{-1}): λ_{max} = 293, 382; ε = 14210, 5263. Anal. Calcd: C, 40.47; H, 4.00; N, 2.78. Anal. Found: C, 40.53; H, 4.02; N, 2.70. ^{1}H NMR (600 MHz, acetone-d_6) δ 1.42−1.89 (m, 11H, Cy), 6.41 (m, 1H), 6.63 (d, 1H, *J* = 8.4 Hz), 7.17 (m, 2H), 8.30 (s, 1H, HC═N). ^{13}C{^{1}H} NMR (600 MHz, acetone-d_6) δ 25.10, 25.67, 26.31, 26.78, 34.55, 35.04, 113.90, 121.99, 122.63, 134.42, 136.47, 163.90, 167.21.

***fac*-[Re(5Me-Sal-3Me2Bu)$(CO)_3$(MeOH)] (6).** The compound was synthesized in a similar fashion as **4** using $[NEt_4]_2[ReBr_3(CO)_3]$ (0.300 g, 0.389 mmol), $AgNO_3$ (0.198 g, 1.168 mmol), and 5Me-SalH-3Me2Bu (0.0840 g, 0.409 mmol). Crystals suitable for X-ray diffraction were obtained at 5 °C. (Yield crystalline product: 0.1278 g, 65%.) IR

dx.doi.org/10.1021/ic5019168 | *Inorg. Chem.* 2014, 53, 12480−12488

(KBr, cm^{-1}): $\nu_{(CO)}$ 2016, 1895, 1872. UV−vis (nm, M^{-1} cm^{-1}): λ_{max} = 382; ε = 1576. Anal. Calcd: C, 40.31; H, 4.38; N, 2.77. Anal. Found: C, 40.37; H, 4.34; N, 2.72. ^{1}H NMR (600 MHz, acetone-d_6) δ 0.95 (m, 3H, CH_3), 1.00 (m, 3H, CH_3), 1.02 (d, 1H, J = 6.8 Hz, CH), 1.06 (d, 1H, J = 6.8 Hz, CH), 1.43 (m, 3H, CH_3), 2.20 (s, 3H, CH_3), 6.25 (dd, 1H, J = 8.0, 1.6 Hz), 6.47 (bs, 1H), 7.04 (t, 1H, J = 8.0 Hz), 8.19 (d, 1H, J = 3.0 Hz). ^{13}C{^{1}H} NMR (600 MHz, acetone-d_6) δ 19.13, 19.57, 21.08, 21.13, 21.79, 34.48, 119.51, 115.60, 122.69, 136.48, 144.97, 164.20, 167.41.

***fac*-[Re(5Me-Sal-*m*Tol)(CO)$_3$(MeOH)] (7).** The compound was synthesized in a similar fashion as **4** using $[NEt_4]_2[ReBr_3(CO)_3]$ (0.300 g, 0.389 mmol), $AgNO_3$ (0.198 g, 1.168 mmol), and 5Me-SalH-*m*Tol (0.0921 g, 0.409 mmol). Crystals suitable for X-ray diffraction were obtained at 5 °C. (Yield crystalline product: 0.2260 g, 60%.) IR (KBr, cm^{-1}): $\nu_{(CO)}$ 2019, 1923, 1883. UV−vis (nm, $M^{-1}cm^{-1}$): λ_{max} = 365; ε = 2124. Anal. Calcd: C, 43.34; H, 3.64; N, 2.66. Anal. Found: C, 43.40; H, 3.60; N, 2.72. ^{1}H NMR (600 MHz, acetone-d_6) δ 2.18 (s, 3H, CH_3), 2.23 (s, 3H, CH_3), 2.35 (s, 3H, CH_3), 2.38 (s, 3H, CH_3), 6.32 (dd, 1H, J = 8.0, 1.5 Hz), 6.44 (m, 1H), 6.56 (s, 1H), 6.62 (s, 1H), 7.16−7.03 (m, 7H), 7.26 (m, 2H), 7.31 (m, 1H), 8.14 (s, 1H), 8.28 (s, 1H). ^{13}C{^{1}H} NMR (600 MHz, acetone-d_6) δ 21.53, 21.90, 116.15, 119.06, 121.44, 123.27, 124.68, 127.23, 136.78, 136.93, 139.02, 145.98, 165.94, 167.72.

X-ray Crystallography. A Bruker X8 ApexII 4K diffractometer[38] (Mo Kα radiation) at 100 K was used to collect diffraction data by ω-and-φ-scans for complexes **5**, **6**, and **7**, as presented in Table 2. To ensure that more than a hemisphere of reciprocal space was collected optimally, the software COSMO[39] was utilized. The integration of the individual frames and data reduction was done using the respective Bruker SAINT-Plus and XPREP[40] software packages, followed by absorption correction using the multiscan technique software SADABS.[41] The direct methods package SIR97[42] was employed to solve the structures, which was subsequently refined using the WinGX[43] software package which incorporates SHELXL.[44] Non-hydrogen atom anisotropic displacement parameter refinement was done, wherein the aromatic and methyl protons were placed in geometrically idealized positions with C−H = 0.98−0.95 Å and U_{iso}(H) = 1.5U_{eq}(C) and 1.2U_{eq}(C), respectively, which were constrained to ride on their respective parent atoms. The methyl H atoms were located from difference Fourier maps, and the group was then refined as a rigid entity. A large net electron density peak/hole is observed approximately 0.8 Å from the Re metal metal center for compound **5** and is assumed to be related to the decomposition of the rhenium salicylidene crystal structure. Molecular structures were obtained using the program DIAMOND,[45] and unless otherwise stated, all structures are presented with thermal ellipsoids at 50% probability level. Hyperchem 7.52 was used to generate overlay illustrations of selected complexes.[46]

Kinetic Studies. Pseudo-first-order conditions, with the ligands in large excess over the metal concentration, were utilized for all kinetic runs. The absorbance versus time data thus obtained from the individual kinetics runs were then subjected to least-squares analyses of the appropriate functions using the program MicroMath Scientist.[47] Experimental values obtained are plotted as individual points denoted by selected symbols, while the solid lines as indicated in the figures represent the least-squares computer fits of data to the appropriate functions. The substitution process of the coordinated methanol by monodentate entering ligands (indicated by L), in the *fac*-[Re(*L*,*L*′-Bid)(CO)$_3$(MeOH)] complexes, is expected to show a concentration dependence of the pseudo-first-order rate constant (k_{obs}) on [L] when described as an interchange process *I*. In this case, the interchange of MeOH and L within the outer-sphere complex ([Re(*L*,*L*′-Bid)(CO)$_3$(MeOH)]···L), as formed in a rapid pre-equilibrium, is followed by a slower rate-determining second reaction as indicated in eq 1.

$$[Re(L,\,L'\text{-Bid})(CO)_3(HOCH_3)] + L \overset{K_2}{\rightleftharpoons} [Re(L,\,L'\text{-Bid})(CO)_3(HOCH_3)]\cdots(L)]$$

$$[Re(L,\,L'\text{-Bid})(CO)_3(HOCH_3)]\cdots(L)] \underset{k_{-3}}{\overset{k_3}{\rightleftharpoons}} [Re(L,\,L'\text{-Bid})(CO)_3(L)] + HOCH_3 \quad (1)$$

Monitoring the kinetics at conditions where [L] ≫ [Re], with typical metal concentrations ranging from 1 × 10^{-4} to 5 × 10^{-4} M, yields the rate equation for this scheme as defined in eq 2.

$$k_{obs} = k_3K_2[L]/(1 + K_2[L]) + k_{-3} \quad (2)$$

Here K_2 is the pre-equilibrium constant, k_3 the observed second-order limiting rate constant, and k_{-3} is the reverse reaction rate constant indicated by the graphical fits of k_{obs} versus ligand concentration.[48,49]

The substitution of methanol in the *fac*-[Re(*L*,*L*′-Bid)(CO)$_3$(MeOH)] complexes for a range of entering ligands can also be defined by the overall equilibrium

$$[Re(L,\,L'\text{-Bid})(CO)_3(HOCH_3)] + L \underset{k_{-1}}{\overset{k_1,K_1}{\rightleftharpoons}} [Re(L,\,L'\text{-Bid})(CO)_3(L)] + HOCH_3 \quad (3)$$

The pseudo-first-order rate constant was obtained from absorbance versus time data to determine the relationship for the profiles wherein linear dependences of k_{obs} versus [Ligand] were observed, as described previously,[20,21] while the overall stability constant (K_1) has been determined kinetically using the definition:

$$K_1 = k_1/k_{-1} \quad (4)$$

The linear concentration dependence of the pseudo-first-order rate constant (k_{obs}) assuming the overall equilibrium defined in eq 3 can be given determined from

$$k_{obs} = k_1[L] + k_{-1} \quad (5)$$

The overall rate equation (eq 5) will only be applicable at low ligand concentrations for the limiting mechanism before saturation limits have been reached, i.e., where linear second-order rate behavior occurs (k_f = k_1 = k_3K_2). The total forward rate constant (k_f) for an interchange mechanism will be similar to the overall second-order rate constant (k_1) within experimental error provided that data from well before the plateau is realized are used. However, at high ligand concentrations, limiting kinetics will dominate, and $k_f \neq k_1$.

■ ASSOCIATED CONTENT

Ⓢ Supporting Information

Tables of additional kinetic data. Crystallographic data in CIF format. This material is available free of charge via the Internet at http://pubs.acs.org. Crystallographic data for the structures **5**, **6**, and **7** are available free of charge from the Cambridge Crystallographic Data Centre via www.ccdc.cam.ac.uk/data_request/cif as CCDC 1015304−1015306.

■ AUTHOR INFORMATION

Corresponding Author

*E-mail: roodta@ufs.ac.za.

Notes

The authors declare no competing financial interest.

■ ACKNOWLEDGMENTS

We gratefully acknowledge financial assistance from the University of the Free State, in particular from the Strategic Academic Research Cluster initiative (the Advanced Biomolecular and the Materials and Nanosciences Clusters, respectively). The South African National Science Foundation

(SA-NRF/THRIP), SASOL, and PETLabs Pharmaceuticals are also acknowledged. Part of this material is based on work supported by the SA NRF/THRIP under Grant GUN 2068915. Opinions, findings, conclusions, or recommendations expressed herein are those of the authors and do not necessarily reflect the views of the SA-NRF/THRIP.

REFERENCES

(1) Koelle, U. *Coord. Chem. Rev.* **1994**, *135*−*136*, 623−650.
(2) Helm, L.; Merbach, A. E. *Chem. Rev.* **2005**, *105*, 1923−1959.
(3) Richens, D. T. *Chem. Rev.* **2005**, *105*, 1961−2002.
(4) Grundler, P. V.; Helm, L.; Alberto, R.; Merbach, A. E. *Inorg. Chem.* **2006**, *45*, 10378−10390.
(5) Safi, B.; Mertens, J.; De Proft, F.; Geerlings, P. *J. Phys. Chem. A* **2006**, *110*, 9240−9246.
(6) Videira, M.; Moura, C.; Datta, A.; Paulo, A.; Santos, I. C.; Santos, I. *Inorg. Chem.* **2009**, *48*, 4251−4257.
(7) Hillard, E. A.; Jaouen, G. *Organometallics* **2011**, *30*, 20−27.
(8) Morais, G. R.; Paulo, A.; Santos, I. *Organometallics* **2012**, *31*, 5693−5714.
(9) Alberto, R.; Schibli, R.; Waibel, R.; Abram, U.; Schubiger, A. P. *Coord. Chem. Rev.* **1999**, *192*, 901−919.
(10) Sulieman, S.; Can, D.; Mertens, J.; N'Dongo, H. W. P.; Liu, Y.; Schmutz, P.; Bauwens, M.; Spingler, B.; Alberto, R. *Organometallics* **2012**, *31*, 6880−6886.
(11) Liu, S. *Chem. Soc. Rev.* **2004**, *33*, 445−461.
(12) Alberto, R. *Eur. J. Nucl. Med. Mol. Imaging* **2003**, *30*, 1299−1302.
(13) Ballinger, J. R.; Cooper, M. S.; Mather, S. J. *Eur. J. Nucl. Med. Mol. Imaging* **2004**, *31*, 304−305.
(14) Liu, S. *Chem. Soc. Rev.* **2004**, *33*, 445−461.
(15) Salignac, B.; Grundler, P. V.; Cayemittes, S.; Frey, U.; Scopelliti, R.; Merbach, A. E. *Inorg. Chem.* **2003**, *42*, 3516−3526.
(16) Grundler, P. V.; Salignac, B.; Cayemittes, S.; Alberto, R.; Merbach, A. E. *Inorg. Chem.* **2004**, *43*, 865−873.
(17) Mundwiler, S.; Kündig, M.; Ortner, K.; Alberto, R. *Dalton Trans.* **2004**, 1320−1328.
(18) Brink, A.; Visser, H. G.; Roodt, A. *J. Coord. Chem.* **2011**, *64*, 122−133.
(19) Brink, A.; Visser, H. G.; Roodt, A. *Polyhedron* **2013**, *52*, 416−423.
(20) Schutte, M.; Kemp, G.; Visser, H. G.; Roodt, A. *Inorg. Chem.* **2011**, *50*, 12486−12498.
(21) Schutte, M.; Roodt, A.; Visser, H. G. *Inorg. Chem.* **2012**, *51*, 11996−12006.
(22) Brink, A.; Visser, H. G.; Roodt, A. *Inorg. Chem.* **2013**, *52*, 8950−8961.
(23) Cotton, F. A.; Wilkinson, G.; Gaus, P. L. *Basic Inorganic Chemistry*, 3rd ed.; John Wiley & Sons Inc.: New York, 1995.
(24) Otto, S.; Roodt, A. *Inorg. Chim. Acta* **2004**, 1−10.
(25) Brink, A.; Roodt, A.; Steyl, G.; Visser, H. G. *Dalton Trans.* **2010**, *39*, 5572−5578.
(26) Roodt, A.; Visser, H. G.; Brink, A. *Crystallogr. Rev.* **2011**, *17*, 241−280.
(27) Faller, J. W.; Mason, G.; Par, J. *J. Organomet. Chem.* **2001**, *626*, 181−185.
(28) Czerwieniec, R.; Kapturkiewicz, A.; Anulewicz-Ostrowska, R.; Nowacki, J. *J. Chem. Soc., Dalton Trans.* **2002**, 3434−3441.
(29) Li, Z. K.; Ki, Y.; Lei, L.; Che, C. M.; Zhou, X. G. *Inorg. Chem. Commun.* **2005**, *8*, 307−309.
(30) Zobi, F.; Spingler, B.; Fox, T.; Alberto, R. *Inorg. Chem.* **2003**, *42*, 2818−2820.
(31) Perrin, D. D. *Dissociation Constants of Organic Bases in Aqueous Solution*; Butterworths: London, 1965; Supplement, 1972.
(32) *CRC Handbook of Chemistry and Physics*, 88th ed. (CD-ROM, Version 2008); Lide, D. R., Ed.; CRC Press/Taylor and Francis: Boca Raton, FL.
(33) Basolo, F.; Pearson, R. G. *Mechanisms of Inorganic Reactions*; John Wiley: New York, 1967.
(34) Alberto, R.; Egli, A.; Abram, U.; Hegetschweiler, K.; Gramlich, V.; Schubiger, P. A. *J. Chem. Soc., Dalton Trans.* **1994**, 2815−2820.
(35) Alberto, R.; Schibli, R.; Schubiger, P. A.; Abram, U.; Kaden, T. A. *Polyhedron* **1996**, *15*, 1079−1089.
(36) Brink, A.; Roodt, A.; Visser, H. G. *Acta Crystallogr.* **2009**, *E65*, o3175−o3176.
(37) Arod, F.; Gardon, M.; Pattison, P.; Chapuis, G. *Acta Crystallogr.* **2005**, *C61*, o317−o320.
(38) *APEX2 (Version 1.0-27)*; Bruker AXS Inc.: Madison, WI, 2005.
(39) *COSMO (Version 1.48)*; Bruker AXS Inc.: Madison, WI, 2003.
(40) *SAINT-Plus (Version 7.12) (including XPREP)*; Bruker AXS Inc.: Madison, WI, 2004.
(41) *SADABS (Version 2004/1)*; Bruker AXS Inc.: Madison, WI, 1998.
(42) Altomare, A.; Burla, M. C.; Camalli, M.; Cascarano, G. L.; Giacovazzo, C.; Guagliardi, A.; Moliterni, A. G. G.; Polidori, G.; Spagna, R. *J. Appl. Crystallogr.* **1999**, *32*, 115−119.
(43) Farrugia, L. J. *J. Appl. Crystallogr.* **1999**, *32*, 837−838.
(44) Sheldrick, G. M. *SHELXL97, Program for Solving Crystal Structures*; University of Göttingen: Germany, 1997.
(45) Brandenburg, K.; Putz, H. *DIAMOND, Release 3.0c*; Crystal Impact GbR: Bonn, Germany, 2005.
(46) *Hyperchem Release 7.52, Windows Molecular Modeling System*; Hypercube, Inc.: Gainesville, FL, 2002.
(47) *Micromath Scientist for Windows, Version 2.01*; MicroMath Inc.: St. Louis, MO, 1995.
(48) Swaddle, T. W. *Adv. Inorg. Bioinorg. Mech.* **1983**, *2*, 95−138.
(49) Wilkins, R. G. *Kinetics and Mechanism of Reactions of Transition Metal Complexes*, 2nd ed.; VCH Publishers, Inc.: New York, 2002.